Ultraviolet observations of the hydrogen coma of comet C/2013 A1 (Siding Spring) by MAVEN/IUVS

Matteo M. J. Crismani, Nicholas M. Schneider, Justin I. Deighan, A. Ian F. Stewart, Michael Combi, Michael S. Chaffin, Nicolas Fougere, Sonal K. Jain, Arnaud Stiepen, Roger V. Yelle, et al.

AGU PUBLICATIONS

Geophysical Research Letters

RESEARCH LETTER
10.1002/2015GL065290

Special Section:
First Results from the MAVEN Mission to Mars

Ultraviolet observations of the hydrogen coma of comet C/2013 A1 (Siding Spring) by MAVEN/IUVS

Matteo M. J. Crismani[1], Nicholas M. Schneider[1], Justin I. Deighan[1], A. Ian F. Stewart[1], Michael Combi[2], Michael S. Chaffin[1], Nicolas Fougere[2], Sonal K. Jain[1], Arnaud Stiepen[1], Roger V. Yelle[3], William E. McClintock[1], John T. Clarke[4], Gregory M. Holsclaw[1], Frank Montmessin[5], and Bruce M. Jakosky[1]

[1]Laboratory for Atmospheric and Space Sciences, University of Colorado Boulder, Boulder, Colorado, USA, [2]Department of Atmospheric, Oceanic, and Space Sciences, University of Michigan, Ann Arbor, Michigan, USA, [3]Lunar and Planetary Laboratory, University of Arizona, Tucson, Arizona, USA, [4]Center for Space Physics, Boston University, Boston, Massachusetts, USA, [5]LATMOS/IPSL, Guyancourt, France

Key Points:
- We determine Comet Siding Spring's water production rate
- We determine the mass of gas that impacted Mars
- We revisit and reconcile predictions with our observations

Correspondence to:
M. M. J. Crismani,
matteo.crismani@colorado.edu

Citation:
Crismani, M. M. J., et al. (2015), Ultraviolet observations of the hydrogen coma of comet C/2013 A1 (Siding Spring) by MAVEN/IUVS, *Geophys. Res. Lett.*, *42*, 8803–8809, doi:10.1002/2015GL065290.

Received 27 JUL 2015
Accepted 30 SEP 2015
Published online 5 NOV 2015

Abstract We used the Imaging Ultraviolet Spectrograph (IUVS) aboard the Mars Atmosphere and Volatile EvolutioN (MAVEN) orbiting spacecraft to construct images of the hydrogen coma of comet C/2013 A1 (Siding Spring) days before its close encounter with Mars. We obtain a water production rate of $1.1 \pm 0.5 \times 10^{28}$ molecules/s and determine the total impacting fluence of atoms and molecules corresponding to the photodissociation of water and its daughter species to be $2.4 \pm 1.2 \times 10^{4}$ kg. We use these observations to confirm predictions that the mass of delivered hydrogen is comparable to the existing reservoir above 150 km. Furthermore, we reconcile disparity between observations and predictions about the detectability of the hydrogen perturbation and thermospheric response.

1. Introduction

The Mars Atmosphere and Volatile EvolutioN (MAVEN) mission is the first to study the evolution of the Martian atmosphere by determining the drivers and effects of atmospheric loss to space [*Jakosky et al.*, 2015]. Although the interaction of Mars and the gaseous coma of a comet, an event predicted to occur only once in 100,000 years [*Ye and Hui*, 2014], was not expected during the MAVEN mission, on 19 October 2014, comet C/2013 A1 (Siding Spring) [*McNaught et al.*, 2013] approached within 141,000 km with a velocity relative to Mars of 56 km/s. Because the delivery of mass and energy from impacting cometary dust and gas is in many ways analogous to impulsive solar events that MAVEN was designed to observe, the spacecraft was well positioned to investigate this rare occurrence.

Some effects of impacting dust have been reported by *Schneider et al.* [2015] and *Benna et al.* [2015], who detected ablated metals in the atmosphere, but the effects of impacting gas are subtler as gaseous species abundant in comets are naturally present in the Mars atmosphere. MAVEN observations of the comet's coma obtained before the closest approach, however, can be used to determine the mass of impacting gas, which is the most critical quantity in interpreting possible impact-related atmospheric changes.

We use direct measurements of the hydrogen brightness distribution and a robust cometary model to determine the comet's water production rate and to quantify the flux of cometary gases on the upper atmosphere. Water is responsible for the majority of the mass in the gaseous coma but is difficult to observe in the UV and visible; we therefore use UV observations of hydrogen as an available proxy.

2. Observations and Data Analysis

Our observations use MAVEN's Imaging Ultraviolet Spectrograph (IUVS), which can derive atmospheric properties through spectroscopic measurements of UV emissions from atmospheric gases [*McClintock et al.*, 2014]. The data are taken in the form of two-dimensional spectrograms, with the horizontal axis corresponding to wavelength, and the vertical axis representing spatial position along the slit, which is 11° tall and 0.06° in the spectral direction. By rotating a scan mirror that moves the position of the slit on the sky, we are able to create data cubes with spatial information on two axes and spectral on the third. We used the far ultraviolet channel that covers wavelengths between 115 and 190 nm and has a spatial resolution along the slit of

Table 1. Information for the Four Observations of Comet C/2013 A1(Siding Spring)[a]

Observation Date and Time (UTC)	Mars-Comet Distance (10^6 km)	Hours Before Closest Approach	Angular Width (deg)	Resolution		Number of Spatial Bins	Projected Spatial Bin Size (km)
				Spectral (nm)	Spatial (″)		
14 Oct 2014 11:33:32[b]	25.56	126.8	2	1.2	96	75	12000
18 Oct 2014 03:02:40[c]	7.95	39.4	2	1.2	190	37	7500
18 Oct 2014 05:20:21[d]	7.54	37.1	2	1.2	190	37	7100
18 Oct 2014 06:00:32[e]	7.34	36.4	10	1.8	190	200	6900

[a]Spatial bins are constructed by binning pixels along the length of the slit, and the spatial resolution below reflects this binning. The data have been publicly archived at the Planetary Atmospheres node of the Planetary Data System (PDS); to retrieve these files, use the filename from footnotes b–e.
[b]mvn_iuv_l1b_APP1-orbit00087-mode0821-fuv_20141014T113335_v02_r01.
[c]mvn_iuv_l1b_comet-orbit00106-mode0021-fuv_20141018T030240_v02_r01.
[d]mvn_iuv_l1b_comet-orbit00106-mode0022-fuv_20141018T052021_v02_r01.
[e]mvn_iuv_l1b_comet-orbit00106-mode0041-fuv_20141018T060032_v02_r01.

0.8 arc min/pixel, a spatial resolution across the slit of 3.6 arc min/pixel, and a spectral resolution of 0.6 nm. Using the Lyman α emission from hydrogen at 121.6 nm, we construct images of the comet by summing over the spectral width of the line and arranging the measurements according to projected positions on the sky. The spectral and spatial binning is shown in Table 1; the projected spatial bin size is a function of the comet's distance from Mars.

IUVS observed Siding Spring once on 14 October 2014 and three times on 18 October 2014. Each observation was composed of 36 scan mirror positions and an integration time of 60 s in each position. Between integrations the line of sight moved by single slit widths (3.6 arc min) perpendicular to the slit's long axis, except for the observation taken on 18 October 2014 06:00:32 UTC, where we moved it by five slit widths (18 arc min) to increase coverage on the sky. The comet was moving almost directly toward Mars at the time of the observations, so despite the high relative velocity (56 km/s), the apparent motion on the sky is negligible compared to the spatial resolution of our images.

Dark frames taken at the beginning and end of each observation were used to subtract dark current. The data were then converted into kilorayleighs per nanometer, a standard unit of brightness used for airglow [*Barth et al.*, 1971]. Stellar calibration was performed using UV bright stars (Bet CMa, Bet Cen, and Alp Cru [*Snow et al.*, 2013]); however, there are differences in our observed brightnesses with previous measurements of the Martian hydrogen corona and interplanetary hydrogen. Comparison with Hubble Space Telescope, and other Lyman α observing instruments, such as Mars Express/SPICAM [*Bertaux et al.*, 2006], SORCE/SOLSTICE [*McClintock et al.*, 2005a, 2005b], and SOHO/SWAN [*Bertaux et al.*, 1995] indicate a discrepancy of order 20%. To account for this, we reduced our intensities with a model-scale factor of ~1.2 as this allows appropriate comparison with other observatories and assigned a 25% systematic error. This affects our retrieved water production rates and inferred masses, as these are directly proportional to the assumed model-scale factor.

The cometary hydrogen signal lies on top of a background from interplanetary hydrogen plus a substantial foreground from the Martian hydrogen corona. We model and subtract these signals to find the distribution of cometary hydrogen across the sky. We use the model described by *Chaffin et al.* [2015], developed for IUVS, to characterize the Martian hydrogen corona; the model of *Lallement et al.* [1985] to compute the interplanetary hydrogen background; and the model of *Tenishev et al.* [2008, and references therein] to model the cometary coma. We simultaneously fit the data to the foreground and radial cometary models by the method of minimum χ^2 and find agreement with nominal coronal parameters within 5%. The foreground signal is the dominant signal in most of the images (Figure 1), and this subtraction leaves a majority of pixels with a uniform uncertainty of ~30%.

The foreground model assumes spherical symmetry, but as described in *Chaffin et al.* [2015], the hydrogen corona is at least slightly asymmetric and this creates an excess of negative values, shown as darker pixels in Figure 1, far from the nucleus (>500,000 km). We exclude distances greater than 200,000 km in this analysis for two reasons: the foreground model is insufficiently precise to distinguish whether the source of this signal is cometary or coronal, and the cometary signal at these distances is so weak that we cannot reliably distinguish it from detector noise. This distinction does not greatly affect the fitting process as the exclusion of data

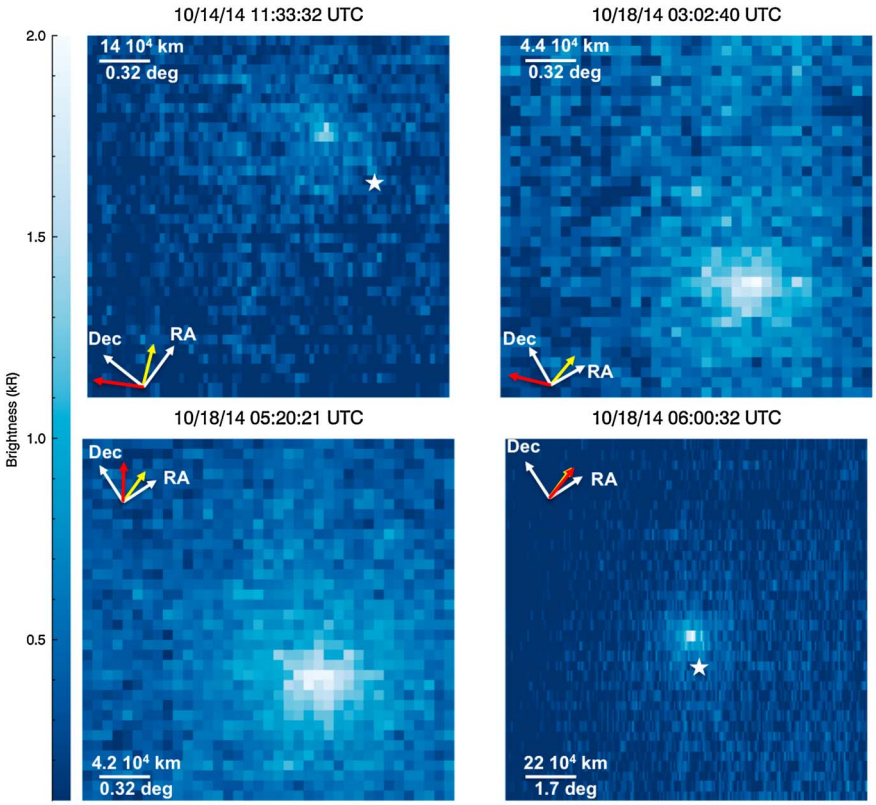

Figure 1. Images of comet A1 C/2013 (Siding Spring), taken on 14 and 18 October, corrected for dark current, foreground, and background signals. A white star shows the approximate location where Mars encountered the gaseous coma. The images are oriented with increasing right ascension and declination aligned along the white arrows. The direction of the Sun and Mars is shown with a yellow and a red arrow, respectively. The slit is aligned horizontally, and the vertical axis spans the range of mirror motion on the sky.

>200,000 km changes the estimated water production rate by 1%. The location of the nucleus is determined by coincidence of the brightest pixel in the image with the ephemeris reported by *JPL* [2015], and from this we produce radial profiles of hydrogen by averaging the data by spatial bins detailed in Table 1, effectively reducing the random uncertainties for each bin to ~5%.

Correcting for the Martian and interplanetary hydrogen components, the measured brightnesses were converted into column densities using the appropriate *g* factor [*Chamberlain and Hunten*, 1990]. The observed radial profile from 14 October 2014 (Figure 2) within 50,000 km deviates from the best fit model, but the inferred water production rate for this observation is within 10% of the subsequent observations, and therefore, we do not include this as a distinct measurement. Due to an incomplete foreground subtraction rather than any cometary effect, the radial profile from 18 October 2014 3:02 UTC is also statistically different from the model at distances greater than 150,000 km, shown as an excess of bright pixels near the top of the second image in Figure 1.

3. Results

3.1. Cometary Gaseous Production

We estimate the total mass of water and its daughter species that impacted Mars using the observations of hydrogen column density from Figure 2. Comparing the measured hydrogen content with a distribution derived from the model of *Tenishev et al.* [2008], we find a water production rate of $1.1 \pm 0.5 \times 10^{28}$ molecules/s and, from this, calculate column densities swept up by Mars during the encounter (Figure 3). The mass from CO_2 delivered to Mars may be an important perturbation to gaseous species in the upper atmosphere, and as CO_2 radial profiles cannot be derived from H, we use reported production rates from *Stevenson et al.* [2015] taken 1 month before the encounter.

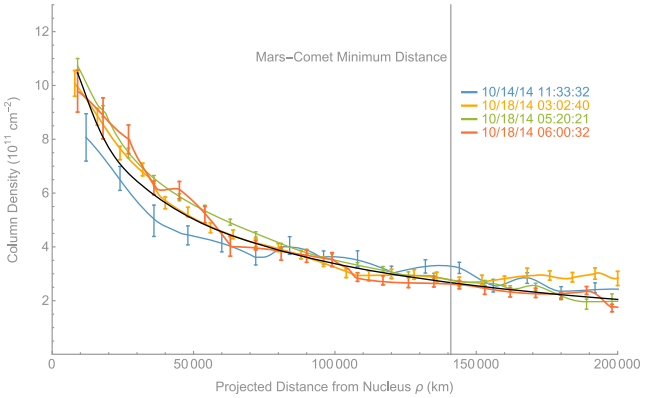

Figure 2. Radial distributions of the observed hydrogen column densities for each of the four observations. Constant width binning of annuli centered on the nucleus produced these azimuthally averaged radial profiles. These observations are fit to a model, described herein, and shown in black. The 1σ error bars represent the variation derived from the photon statistics of the detector.

We predict column densities of water and its daughter species using a fully kinetic Adaptive Mesh Particle Simulation model [*Tenishev et al.*, 2008; *Combi et al.*, 2012; *Fougere*, 2014; *Fougere et al.*, 2012, 2013]. This enables us to model the full coma of Siding Spring, including regions where collisions are not sufficient to maintain a fluid regime. This technique uses the gaseous production rate and heliocentric distance as inputs and produces radial profiles that we compare against observations. Systematic differences among various measures of water production rates normally fall in the range of 25–50%, owing to differences in calibration, background subtraction, model assumptions, and model parameter uncertainties, and we adopt a conservative systematic uncertainty of 50%. Although the model used includes the expected detailed spatial and velocity distributions of H atoms produced by photodissociation of H_2O and OH, a simple Haser model with an average radial velocity yields a consistent result to well within the measurement uncertainty.

The sublimation of water and subsequent photodissociation into OH, O, and H described by this model infer fluxes of mass and energy as shown in Table 2. The H profile results from the progressive dissociation of H_2O and OH into its constituent atoms which happens continuously as the gases flow outward. Our results broadly agree with the work of *Bodewits et al.* [2015], with differences in relative abundance of daughter species due to a difference in modeling methods: spherically symmetric radial outflow Haser model [see *Bodewits et al.*, 2011] versus direct simulation modeling, presented here. As ionization and chemical processes will affect these species during deposition, this discrepancy is unlikely to be discernible in subsequent atmospheric observation.

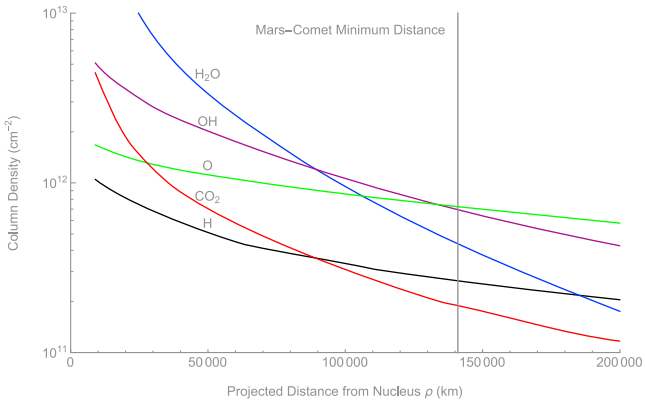

Figure 3. Modeled line of sight column densities the major gaseous species derived from the model of *Tenishev et al.* [2008]. The black line shown here for hydrogen corresponds to the same line in Figure 2, but the vertical scale is now logarithmic.

Table 2. Impacting Fluence of Mass and Energy for Gaseous Species From Comet Siding Spring[a]

	Particle Flux (10^7 cm^{-2} s^{-1})	Column Energy Density (erg cm^{-2})	Mass (kg)
H	7	7	160
O	20	300	6900
OH	19	310	7000
H_2O	12	200	4600
CO_2[b]	5	210	4900
Total		1,000	24,000

[a]The fluxes are determined using the total impacting model column densities by species averaged over the encounter, where we used a nominal encounter time of 60 min [see *Yelle et al.*, 2014 for details]. Values derived from water are valid within 50% (see text for discussion).
[b]Derived from CO_2 production rate of *Stevenson et al.* [2015].

The radial profiles we obtained days in advance of the encounter can be used to estimate the impacting gas mass at the time of closest approach, on the assumption that the profile is steady state, smoothly varying and azimuthally symmetric. The region of interest in the gaseous coma lies far enough from the comet that asymmetries due to ejection and rotational variations are smoothed, but close enough that radiation pressure does not appreciably affect the coma [*Combi et al.*, 2000]. Given the small change in heliocentric distance over this time span, no significant temporal variability of sublimation or dissociation is expected.

3.2. Martian Atmospheric Effects

The total mass of impacting gas is $2.4 \pm 1.2 \times 10^4$ kg and is larger than the total impacting dust mass determined by *Schneider et al.* [2015], which was between 2700 and 16,000 kg. However, cometary gases shown in Table 2 are unlikely to cause significant mass perturbations in the upper atmosphere. Molecules are expected to dissociate upon entry into the upper atmosphere, and we can compare the combined mass of O, C, and H from all parents to the ambient density at the predicted penetration depth (~154 km [*Yelle et al.*, 2014]). The observed cometary oxygen column is equivalent to the amount of oxygen in a 200 m layer of Mars atmosphere at 155 km [*Bougher et al.*, 2015]. Compared to the mass of oxygen above this altitude, we find this is a perturbation of order 1% and, so far, unobservable in the IUVS atmospheric data. As carbon dioxide and carbon monoxide are dominant species in the Martian atmosphere, cometary perturbations to these species are unlikely to be detectable. However, atomic and ionized carbon densities are extremely reduced in comparison, and analysis is underway to determine whether perturbations to carbon are observable by IUVS. The majority of cometary hydrogen delivered to Mars comes from dissociation of H_2O and OH upon entry into the atmosphere, and the delivery from atomic hydrogen is ~6 times smaller. Cometary hydrogen delivered to the planet from water and its products is $3.4 \pm 1.7 \times 10^{12}$ atoms/cm^2 which is comparable to, but smaller than, the abundance of hydrogen at Mars above 150 km [*Krasnopolsky*, 2002; *Chaufray et al.*, 2008]. However, this mass perturbation is difficult to find in subsequent atmospheric observations as the Lyman α emission from hydrogen is optically thick and doubling the density does not double the observed brightness.

These observations and analysis of early atmospheric data from IUVS allow us to determine the energy delivered to the upper atmosphere and its penetration depth. Water traveling at the relative speed of 56 km/s carries a kinetic energy of 293 eV/molecule and will deposit oxygen and hydrogen in the upper atmosphere as it is stopped by collisions with ambient species. For a water production rate of 10^{28} molecules/s *Yelle et al.* [2014] predicted impacting water and its daughter species should increase the temperature in the upper atmosphere by 30 K. Temperatures derived from observed typical scale heights from IUVS limb scans [*Jain et al.*, 2015] before the comet encounter indicate the atmospheric temperature may be 100 K larger than those assumed by *Yelle et al.* [2014]. The penetration depth is sensitive to the assumed atmospheric temperature and this disparity indicates the thermospheric effect would have occurred ~20 km higher than predicted. Further analysis will be necessary to determine whether IUVS is able to detect this 10% perturbation as the work by *Jain et al.* [2015] uses an exponential fit to derive scale heights, and ongoing analysis will be able to produce temperature that is resolved in altitude.

4. Conclusions

Measurements of the hydrogen coma density allow us to infer the water production rate for comet Siding Spring before its close encounter with Mars. We find a water production rate of $1.1 \pm 0.5 \times 10^{28}$ molecules/s by fitting observed radial profiles to predictions from a robust cometary model. From this value, we are able to determine the total mass of gaseous material that impacted Mars from water and its daughter species. We use inferred impacting gaseous masses to revisit and reconcile predictions, finding agreement that the oxygen perturbation is negligible, prompting further work in the analysis of carbon, and determining that the hydrogen perturbation would be unobservable in the IUVS data. The prediction of a thermospheric response due to energy deposition in the upper atmosphere is unchanged by these findings; however, we posit that such perturbations should exist at higher altitudes due to the difference between observed and predicted atmospheric temperatures above 150 km, and analysis is underway to resolve this perturbation if it exists.

Acknowledgments
The data have been publicly archived at the Planetary Atmospheres node of the Planetary Data System (PDS). The MAVEN project is supported by NASA through the Mars Exploration Program. Combi and Fougere acknowledge support from NASA Planetary Atmospheres grant NNX14AG84G, Chaffin acknowledges support from NESSF grant 11-Planet11F-0060, and Stiepen is supported by the Belgian American Educational Foundation and the Rotary District 1630. The authors thank Dennis Bodewits for his helpful discussion.

References

Barth, C., C. Hord, J. Pearce, K. Kelly, G. Anderson, and A. Stewart (1971), Mariner 6 and 7 ultraviolet spectrometer experiment: Upper atmosphere data, *J. Geophys. Res.*, *76*(10), 2213–2227.

Benna, M., P. Mahaffy, J. Grebowsky, J. Plane, R. Yelle, and B. Jakosky (2015), Metallic ions in the upper atmosphere of Mars from the passage of comet C/2013 A1 (Siding Spring), *Geophys. Res. Lett.*, *42*, 4670–4675, doi:10.1002/2015GL064159.

Bertaux, J., et al. (1995), SWAN: A study of solar wind anisotropies on SOHO with Lyman alpha sky mapping, *Sol. Phys.*, *162*(1–2), 403–439.

Bertaux, J.-L., et al. (2006), SPICAM on Mars Express: Observing modes and overview of UV spectrometer data and scientific results, *J. Geophys. Res.*, *111*, E10S90, doi:10.1029/2006JE002690.

Bodewits, D., G. Villanueva, M. Mumma, W. Landsman, J. Carter, and A. Read (2011), Swift-UVOT grism spectroscopy of comets: A first application to C/2007 N3 (Lulin), *Astron. J.*, *141*(1), 12.

Bodewits, D., M. S. Kelley, J.-Y. Li, T. L. Farnham, and M. F. A'Hearn (2015), The pre-perihelion activity of dynamically new comet C/2013 A1 (Siding Spring) and its close encounter with Mars, *Astrophys. J. Lett.*, *802*(1), L6.

Bougher, S., D. Pawlowski, J. M. Bell, S. Nelli, T. McDunn, J. R. Murphy, M. Chizek, and A. Ridley (2015), Mars Global Ionosphere-Thermosphere Model: Solar cycle, seasonal, and diurnal variations of the Mars upper atmosphere, *J. Geophys. Res. Planets*, *120*, 311–342, doi:10.1002/2014JE004715.

Chaufray, J.-Y., J.-L. Bertaux, F. Leblanc, and E. Quémerais (2008), Observation of the hydrogen corona with SPICAM on Mars Express, *Icarus*, *195*(2), 598–613.

Chaffin, M. S., J.-Y. Chaufray, I. Stewart, F. Montmessin, N. M. Schneider, and J.-L. Bertaux (2014), Unexpected variability of Martian hydrogen escape, *Geophys. Res. Lett.*, *41*, 314–320, doi:10.1002/2013GL058578.

Chaffin, M. S., et al. (2015), Three dimensional structure of the Mars H corona revealed by IUVS on MAVEN, *Geophys. Res. Lett.*, *42*, doi:10.1002/2015GL065287.

Chamberlain, T. P., and D. M. Hunten (1990), *Theory of Planetary Atmospheres: An Introduction to Their Physics and Chemistry*, vol. 36, Academic Press, New York.

Combi, M., A. Reinard, J.-L. Bertaux, E. Quemerais, and T. Mäkinen (2000), SOHO/SWAN observations of the structure and evolution of the hydrogen Lyman-α coma of Comet Hale–Bopp (1995 O1), *Icarus*, *144*(1), 191–202.

Combi, M., V. Tenishev, M. Rubin, N. Fougere, and T. I. Gombosi (2012), Narrow dust jets in a diffuse gas coma: A natural product of small active regions on comets, *Astrophys. J.*, *749*(1), 29.

Fougere, N. (2014), The complex outgassing of comets and the resulting coma a direct simulation Monte-Carlo approach, PhD thesis, Univ. of Mich., Ann Arbor.

Fougere, N., M. Combi, V. Tenishev, M. Rubin, B. Bonev, and M. Mumma (2012), Understanding measured water rotational temperatures and column densities in the very innermost coma of Comet 73P/Schwassmann–Wachmann 3 B, *Icarus*, *221*(1), 174–185.

Fougere, N., M. Combi, M. Rubin, and V. Tenishev (2013), Modeling the heterogeneous ice and gas coma of Comet 103P/Hartley 2, *Icarus*, *225*(1), 688–702.

JPL (2015), Horizons database. [Available at http://ssd.jpl.nasa.gov/horizons.cgi, May 2015.]

Jain, S. K., et al. (2015), Preliminary analysis of Martian dayglow observed by the Imaging Ultraviolet Spectrograph aboard MAVEN, *Geophys. Res. Lett.*, *42*, doi:10.1002/2015GL065419.

Jakosky, B. M., et al. (2015), The Mars Atmosphere and Volatile EvolutioN (MAVEN) mission, *Space Sci. Rev.*, doi:10.1007/s11214-015-0139-x.

Krasnopolsky, V. A. (2002), Mars' upper atmosphere and ionosphere at low, medium, and high solar activities: Implications for evolution of water, *J. Geophys. Res.*, *107*(E12), 5128, doi:10.1029/2001JE001809.

Lallement, R., J. Bertaux, and F. Dalaudier (1985), Interplanetary lyman-alpha spectral profiles and intensities for both repulsive and attractive solar force fields predicted absorption pattern by a hydrogen cell, *Astron. Astrophys.*, *150*, 21–32.

McClintock, W. E., M. Snow, and T. N. Woods (2005a), Solar-Stellar Irradiance Comparison Experiment II (SOLSTICE II): Pre-launch and on-orbit calibrations, *Sol. Phys.*, *230*(1–2), 259–294.

McClintock, W. E., G. J. Rottman, and T. N. Woods (2005b), Solar-STELLAR IRRADIANCE COMPARISON EXPERIMENT II (SOLSTICE II): Instrument concept and design, *Sol. Phys.*, *230*, 225–258.

McClintock, W. E., N. M. Schneider, G. M. Holsclaw, J. T. Clarke, A. C. Hoskins, I. Stewart, F. Montmessin, R. V. Yelle, and J. Deighan (2014), The Imaging Ultraviolet Spectrograph (IUVS) for the MAVEN mission, *Space Sci. Rev.*, 1–50, doi:10.1007/s11214-014-0098-7.

McNaught, R., H. Sato, and G. Williams (2013), *Comet C/2013 A1 (Siding Spring)*, 1, vol. 3368, Central Bureau Electronic Telegrams, Cambridge, Mass.

Schneider, N., et al. (2015), MAVEN IUVS observations of the aftermath of the comet Siding Spring meteor shower on Mars, *Geophys. Res. Lett.*, *42*, 4755–4761, doi:10.1002/2015GL063863.

Snow, M., A. Reberac, E. Quémerais, J. Clarke, W. McClintock, and T. Woods (2013), A new catalog of ultraviolet stellar spectra for calibration, in *Cross-Calibration of Far UV Spectra of Solar System Objects and the Heliosphere*, edited by E. Quémerais, M. Snow, and R.-M. Bonnet, pp. 191–226, Springer, New York.

Stevenson, R., J. Bauer, R. Cutri, A. Mainzer, and F. Masci (2015), NEOWISE observations of comet C/2013 A1 (Siding Spring) as it approaches Mars, *Astrophys. J. Lett.*, *798*(2), L31.

Tenishev, V., M. Combi, and B. Davidsson (2008), A global kinetic model for cometary comae: The evolution of the coma of the Rosetta target comet Churyumov-Gerasimenko throughout the mission, *Astrophys. J.*, *685*(1), 659.

Ye, Q.-Z., and M.-T. Hui (2014), An early look of comet C/2013 A1 (Siding Spring): Breathtaker or nightmare?, *Astrophys. J.*, *787*(2), 115.

Yelle, R. V., A. Mahieux, S. Morrison, V. Vuitton, and S. Hörst (2014), Perturbation of the Mars atmosphere by the near-collision with Comet C/2013 A1 (Siding Spring), *Icarus*, *237*, 202–210.